Endogenous Nonionic Saturated Monoethanolamide Lipids: Solid State, Lyotropic Liquid Crystalline, and Solid Lipid Nanoparticle Dispersion Behavior

Sharon M. Sagnella,[†] Charlotte E. Conn,[‡] Irena Krodkiewska,[‡] Minoo Moghaddam,[†] and Calum J. Drummond*[,‡,§]

CSIRO Molecular and Health Technologies, P.O. Box 184, North Ryde, New South Wales 1670, Australia, CSIRO Molecular and Health Technologies, Private Bag 10, Clayton, Victoria 3169, Australia, and CSIRO Materials Science and Engineering, Bag 33, Clayton South, Victoria 3169, Australia

Received: November 5, 2009; Revised Manuscript Received: December 20, 2009

The *n*-acylethanolamides (NAEs) are a family of naturally occurring monoethanolamide containing lipids that display a variety of interesting biological properties. In this study, some physicochemical properties of a series of saturated monoethanolamide lipids with increasing hydrocarbon chain length (lauroyl, myristoyl, palmitoyl, and stearoyl) have been investigated. Temperature induced phase transitions for these NAEs indicate that both the monoethanolamide headgroups and the unsaturated hydrophobic tails play a role in the melting behavior of these lipids. All four lipids examined demonstrate the presence of at least three different polymorphic crystal forms. Transitions in crystal structure can be induced via heating and visualized with polarized optical microscopy. At room and physiological temperature, the four NAEs are solid lamellar crystalline materials. All four molecules form lyotropic liquid crystalline phases in water, albeit at relatively high temperatures, including the lamellar liquid crystalline phase and at least two isotropic phases. Lamellar crystalline palmitoyl monoethanolamide was dispersed as solid lipid nanoparticles (SLNs). The cytotoxicity of these SLNs toward human mammary epithelial cells (HMEpiC) and the MCF7 breast cancer cell line was assessed at physiological temperature. The palmitoyl monoethanolamide SLNs showed little to no toxicity to the HMEpiC even at a concentration of 30 μM. At concentrations above 3 μM, the HMEpiC population was reduced by less than 15%, while the MCF7 population was reduced by $\sim$20−30%. The endogenous nature and natural medicinal properties make this series of lipids ideal candidates for further investigation as solid lipid nanoparticle drug delivery systems.

Introduction

The rational design of novel fit-for-purpose amphiphiles requires an understanding of relationships between structure, composition, and function. A considerable amount of attention has been given to the investigation of phase behavior for amphiphilic lipids.[1−3] In many cases, these studies have been conducted to gain a better understanding of the lipid's role in biomembranes. However, more recently, other areas such as controlled drug delivery,[4,5] nucleic acid delivery,[6,7] and membrane protein crystallization[8−10] have begun to direct more focus on amphiphile phase behavior and concomitant self-assembly materials. Given that an amphiphile has a molecular structure that lends itself to self-assembly in an aqueous environment, the local constraints imposed by the effective shape of the molecule combined with the influence imposed by the competing interactions of the polar headgroups and the alkyl chains govern low volume fraction phase behavior. The type of phase formed can be estimated by utilizing the critical packing parameter (CPP $= v/(l_c a_0)$), where l_c is the effective length of an amphiphile chain, a_0 is the effective amphiphile headgroup area, and v is the average volume occupied by the amphiphile chain.[11] Thus, an amphiphile with a fluid chain and CPP $\approx$ 1 favors the formation of a liquid crystalline lamellar (L_α) phase, which consists of a one-dimensional stack of flat amphiphilic bilayers separated by water layers and forms the basic building block of biological membranes. As the molecule acquires a more reverse wedge-shape, there is an increased desire for curvature and the formation of inverse mesophases such as inverse bicontinuous cubic phases (Q_{II}) and the inverse hexagonal phase (H_{II}) may be favored. An extremely high desire for curvature may result in the formation of inverse micelles where the hydrophilic headgroups are arranged toward water cores with hydrophobic chains radiating outward. These micelles may be arranged in an entirely disordered manner resulting in a fluid inverse micellar phase, the L_2 phase.[12−14] Intermediate and swollen spongelike phases have also been identified in some nonlamellar forming lipid systems.[15−17]

Intermolecular forces also have an important role in determining the structure and morphology of self-assembly structures. For instance, intermolecular hydrogen bonding through the headgroup effectively decreases the hydrophilicity of the headgroup, thereby decreasing headgroup area. In a number of cases, this prompts the formation of inverse phases since a reversed curvature will minimize the distance between headgroups, thus facilitating H-bonding.[12,18] A number of factors relating to the effective volume of the hydrocarbon chain can affect mesophase formation. Intrinsic differences in chain morphology, for example, the introduction of *cis*-double bonds or branching into single chain amphiphiles, can promote the formation of inverse phases by increasing hydrophobic tail volume.[13,14,19] Moreover, increasing the number of hydrophobic

* Corresponding author. E-mail: calum.drummond@csiro.au. Telephone: +61 3 9545 2050. Fax: +61 3 9545 2059.
[†] CSIRO Molecular and Health Technologies, New South Wales.
[‡] CSIRO Molecular and Health Technologies, Victoria.
[§] CSIRO Materials Science and Engineering.

10.1021/jp910578h
Published on Web 01/11/2010

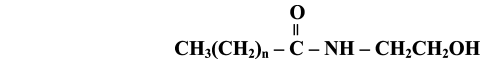

Figure 1. Structure of monoethanolamide lipids where $n = 10$, 12, 14, and 16 for lauoryl, myristoyl, palmitoyl, and stearoyl, respectively.

tails can have the same effect. For instance, double chain amphiphiles containing two long saturated chains can induce inverse phase formation.[12,18,20] Additionally, extrinsic factors such as changes in temperature and pressure can affect mesophase behavior. Increases in temperature can cause hydrophobic chain melting, resulting in an increase in chain fluidity and an effective increase in the chain volume due to an increase in the conformational fluctuations.[12] Thus, by taking all of these aspects of an amphiphile into account, we can begin to design or choose existing amphiphiles based on their structure to fulfill a desired application.

The *n*-acylethanolamides (NAEs) are an interesting family of naturally occurring amphiphilic molecules present in both plant and animal tissues.[21−26] The NAEs consist of both unsaturated chain and saturated chain monoethanolamides and have been shown in numerous studies to exhibit biological and medicinal properties. In the case of the saturated NAEs, stearoyl monoethanolamide (SEA) is produced in several different mammalian tissues, has been shown to induce apoptosis in rat C6 glioma cells,[27] may be important in response to severe inflammation,[28] and has been shown to exert an anorexic effect in mice.[29] Palmitoyl monoethanolamide (PEA) has been implicated in pain suppression and antiepileptic function.[18,30,31] Furthermore, lauroyl and myristoyl monoethanolamide (LEA, MEA), identified in plant tissues, have been shown to accumulate in tobacco cells in response to a fungal elicitor[32] but have not yet been studied for biological function in human cells.

Despite the body of work that has been performed in relation to the biological and pharmacological properties of NAEs, very few studies have investigated the physiochemical properties of these molecules. A series of studies by Ramakrishnan and coworkers examined the thermal phase transitions of dry and hydrated forms of even and odd chain length NAEs via differential scanning calorimetry.[22,23] In addition, X-ray crystallographic studies have examined the molecular packing of MEA, PEA, and SEA.[24,32,33] Recently, we have investigated the neat and lyotropic phase behavior of unsaturated and isoprenoid type monoethanolamide amphiphiles.[13,14]

Both lyotropic liquid crystalline mesophases and dispersions of solid lipid nanoparticles can provide matrices for sustained drug release.[4,34,35] Due to their therapeutic properties and their endogenous nature, this series of monoethanolamide lipids make ideal candidates for study in drug delivery applications. Here, we have investigated the solid state and lyotropic liquid crystalline phase behavior of *n*-lauroyl (C12), *n*-myristoyl (C14), *n*-palmitoyl (C16), and *n*-stearoyl (C18) monoethanolamide (Figure 1). In particular, we describe the thermal properties of the neat materials, crystalline structure of the neat lipids, and the lyotropic phase behavior of these four lipids in water. Additionally, we have dispersed palmitoyl monoethanolamide into a stable, uniform population of solid lipid nanoparticles and have examined the toxicity of these particles to both human mammary epithelial cells and MCF7 breast cancer cells.

Experimental Methods

Materials. All reagents for synthesis were obtained from Sigma-Aldrich, and organic solvents were either of analytical or spectroscopic grade and used as received. Deionized tap water was filtered via a Milli-Q Plus Ultrapure water system (Millipore; Australia) to obtain high purity water.

Monoethanolamide Lipid Synthesis. Monoethanolamide lipids were prepared as described previously.[13,14] Briefly, the desired fatty acid (C12−C18) was dissolved in dichloromethane (DCM) and placed in a round-bottom flask. The resulting solution was placed in an ice bath and stirred vigorously followed by the addition of 2 mol equiv of oxalyl chloride. The reaction was stirred for 10 min in the ice bath. The flask was then sealed, and the atmosphere was evacuated under vacuum and replaced with nitrogen. The reaction was stirred for 2 h at room temperature under nitrogen. At the end of 2 h, the excess oxalyl chloride was evaporated. The resulting fatty acid chloride was dissolved in DCM and slowly added dropwise into ethanolamine (2 mol equiv) in DCM. The reaction was maintained in an ice bath with rapid stirring. After 10 min, the reaction was sealed, the atmosphere was evacuated, and nitrogen was added. The flask was returned to the ice bath and left to react with stirring for 2 h. The resulting product was filtered twice using Whatman 542 filter paper. The filtered solution was then sequentially rinsed with 4% citric acid, 4% sodium bicarbonate solution, and Milli-Q water. DCM was then evaporated under vacuum, leaving white powder for all four lipids. HPLC, NMR, and LC/MS were used to assess the purity of the monoethanolamide lipids, and all compounds had >99.5% purity.

Differential Scanning Calorimetry (DSC). DSC was performed using a Mettler DSC822^e system with a Mettler TSO 801RO sample robot (Mettler Toledo; Melbourne, Australia). Samples were run at three different scan rates: 10, 2.5, and 0.1 °C/min. Data were collected using the STARe software package (Mettler Toledo; Melbourne, Australia). Temperature calibration (±0.3 °C) of the ceramic sensor was performed using octane, water, indium, and zinc. Thermal calibration was performed via integration of a standard indium peak. The energies and peak temperatures of the endotherms of the monoethanolamide lipids were determined using the STARe software package.

Water Penetration into Saturated Monoethanolamide Lipids. Crystalline monoethanolamide amphiphile was placed onto a microscope slide and heated to melting. A coverslip was placed on top of the melted lipid, and the lipid was then cooled to room temperature. A small drop of water placed at the edge of the coverslip was drawn between the two glass surfaces via capillary action to surround the crystalline material. The microscope slide was placed into a Linkam PE94 hot stage (Linkam Scientific Instruments Ltd.; Surry, England) and heated at 1 °C/min or less. An Olympus GX51 inverted optical microscope (Olympus Australia Pty. Ltd.; Melbourne, Australia) both with and without cross polarizing lenses was used to observe the water/monoethanolamide lipid interface. Images were captured with an Olympus c-5060 digital camera (Olympus Australia Pty. Ltd.; Melbourne, Australia).

Binary Phase Behavior of Saturated Monoethanolamide Lipids. Monoethanolamide amphiphile/water mixtures were prepared by weighing out a specific amount of the monoethanolamide lipid into glass ampules. Water was then added to the ampule to create samples ranging from 5 wt % lipid in water to 95 wt % lipid in water. The glass ampules were sealed, and the lipid/water mixture was subjected to heating followed by rapid cooling in order to initially dissolve the lipids. Samples were then submerged into a glass water bath with cross polarizing film attached. The water temperature was controlled and monitored by using a polystat cc1 water bath heater (Crown Scientific Pty. Ltd.; Sydney, Australia) equipped with an internal

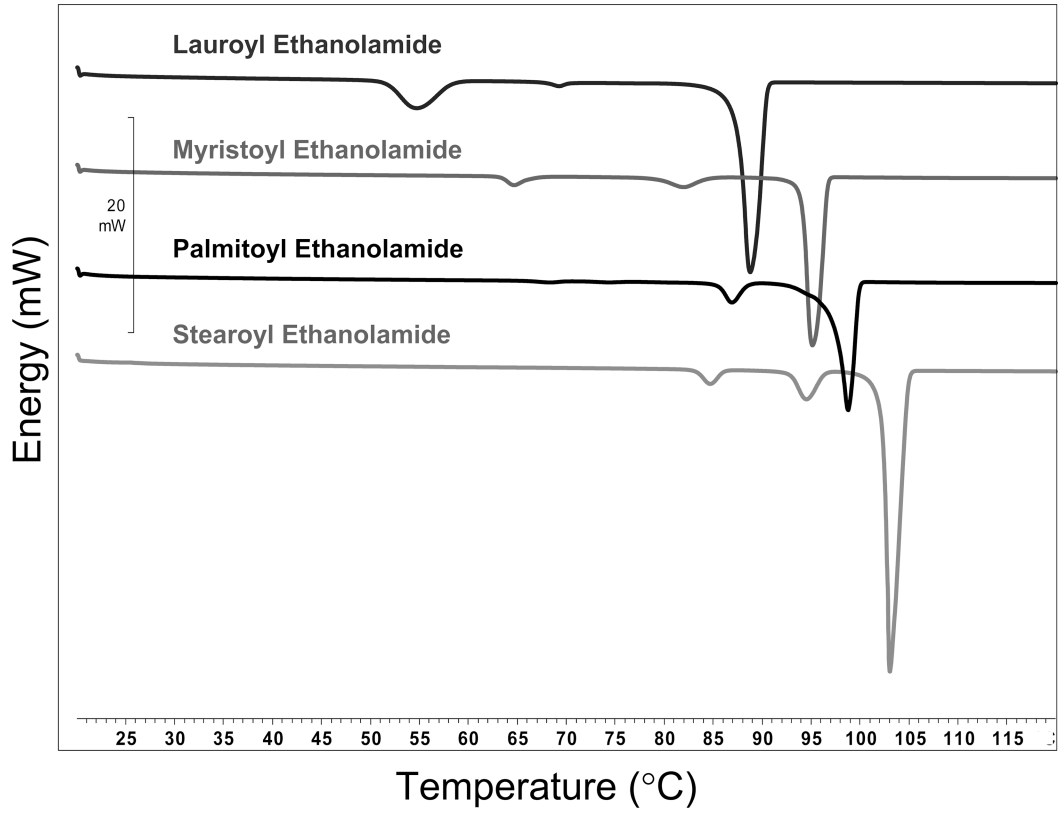

Figure 2. Differential scanning calorimetry traces for stearoyl monoethanolamide, palmitoyl monoethanolmaide, myristoyl monoethanolamide, and lauroyl monoethanolamide. Scan rate = 2.5 °C/min.

TABLE 1: Neat Saturated Monoethanolamide Lipid Phase Transition Data Determined from DSC Scanned at 2.5 °C/min[a]

surfactant	transition temperatures (°C)	transition enthalpy (kJ/mol)	melting point (°C)
stearoyl monoethanolamide	(84), (94), 103	(−2.8), (−6.8), −54.2	102.8 ± 0.5
palmitoyl monoethanolamide	(76), (87), 99.1	(−0.22), (−9.2), −46.4	99.2 ± 0.4
myristoyl monoethanolamide	(64), (77), 95.1	(−2.7), (−8.6), −43.8	95.1 ± 0.1
lauroyl monoethanolamide	(55), (72), 88.8	(−9.5), (−0.44), −34.0	88.9 ± 0.5

[a] Values in parentheses refer to a transition that occurs before the crystal−isotropic liquid transition. Melting point determined by visual inspection.

digital thermometer. The temperature was incrementally increased and held constant to allow for equilibration of samples at desired temperatures. Samples were illuminated and examined through the cross polarizing filters to determine phase transitions.

X-ray Diffraction (XRD). XRD analyses were performed on a PANalytical X'pert PRO X-ray diffractometer. Incident X-ray radiation was produced from a line-focused PW3373/00 Cu X-ray tube operating at 45 kV and 40 mA. The solid sample was placed and pressed into a circular metal sample holder. The sample stage was Spinner PW3064 with reflection but not moving. The diffracted beam produced by interaction with the sample was detected by an X'Pert data collector. Samples were analyzed at room temperature over a range of 2−60° 2θ with a step size of 0.05° 2θ, with each step measured for 60 s.

Solid Lipid Nanoparticle Dispersions. Solid lipid nanoparticle (SLN) dispersions of palmitoyl monoethanolamide were prepared as follows. The steric stabiliser F127 (0.75% w/w; Sigma-Aldrich) was first dissolved in water, and then 10% w/w lipid was added to the solution. The lipid/polymer solution was mixed at elevated temperature under shear using an Ultraturrax homogenizer for 5 min. The coarse dispersion was rapidly transferred to a high pressure homogenizer (Avestin C5) and subjected to recirculation at 170 MPa (25000 psi) for 30 min. Samples were then left to cool for at least 2 h. Once the dispersion was cooled to room temperature, the particle size was measured using a Malvern Zetasizer Nano ZS (Malvern Instruments; Sutherland, Australia).

Cryo-transmission electron microscopy (TEM) was employed to visualize the nanostructure of the dispersed particles. A laboratory-built vitrification system which allowed the humidity to be kept close to 90% during sample plunging and vitrification was used for sample preparation. A 4−5 μL drop of the dispersion was placed on a perforated carbon coated TEM grid and gently blotted with filter paper to obtain a thin liquid film (20−400 nm). The grid was then quickly plunged into liquid ethane at −180 °C and transferred into liquid nitrogen (−195 °C). The sample was then transferred to a cryo-TEM (TECNAI 30 or TECNAI 12) instrument operating at 120 kV. The working temperature was kept below −180 °C and standard low-dose procedures were used to minimize radiation damage. Images were acquired digitally with a MegaView III CCD camera.

Cell Culture. Two cell types were utilized for the cytotoxicity studies: normal human mammary epithelial cells (HMEpiC, primary cell purchased from ScienCell, USA) and MCF7 (breast cancer) cells. HMEpiC were routinely subcultured and grown to confluence from a 1:3 split via trypsinization in 75 cm^2 flasks coated with human fibronectin (1 μg/cm^2; Invitrogen) in HuMEC serum free medium with 0.01% HuMEC supplement and 0.05% bovine pituitary extract (Invitrogen). MCF7 cells were subcultured and grown to ∼85% confluence from a 1:10 split in 75

cm^2 flasks in RPMI 1640 medium containing 10% fetal bovine serum (Invitrogen).

In order to examine the antiproliferative activity of the palmitoyl monoethanolamide SLNs, HMEpiC were seeded onto 96-well microtest plates coated with human fibronectin (1 $\mu g/cm^2$), while MCF7 cells were seeded onto uncoated plates, both at a concentration of ~10 000 cells/well. Cells were left to attach and grow for 48 h, at which time 10 μL of SLN dispersions were added at a concentration ranging from 0.003 to 30 mM. The cells were incubated with the SLNs for another 48 h, and the toxicity of the SLNs was determined by measuring the conversion of a tetrazolium compound into a formazan product by the mitochondria of living cells (CellTiter 96 AQ_{ueous} One Solution Cell Proliferation Assay, Promega, Australia). After 2−4 h incubation with the reagent, the absorbance was measured with a Wallac Victor 1420 multilable counter at $\lambda = 490$ nm (Perkin-Elmer Life Science).

Results and Discussion

Differential Scanning Calorimetry. DSC scans run at 2.5 °C/min for each of the monoethanolamide lipids are shown in Figure 2. DSC scans run at 10 °C/min (not shown) were started at −130 °C, and no additional peaks were observed at temperatures below those shown in Figure 2. Table 1 displays the melting point transition temperatures and enthalpies for the transitions, along with melting points obtained from visual observations. Transition temperatures were obtained from the peak maxima of the endotherms. Enthalpies were obtained by integration of the transition peaks.

The melting points for the monoethanolamide lipids increased with increasing hydrocarbon chain length. The extent of increase, however, becomes less pronounced for longer hydrocarbon chains. A similar trend for NAEs with even hydrocarbon chain lengths was reported by Ramakrishnan et al.[22] This result indicates that the melting behavior is strongly influenced by the hydrocarbon chain; similar to what has been reported for the analogous fatty acids. The crystal−isotropic liquid transition melting temperatures obtained by visual inspection were in agreement with those recorded by DSC.

The transition enthalpy of melting for all four monoethanolamide lipids is of similar magnitude. This may be indicative of the fact that these molecules pack in a similar fashion in the solid and liquid state. The enthalpy values obtained in this study were similar in magnitude to those reported by Ramakrishnan et al. but did not show the same linear dependence on chain length.[22] We do, however, observe an increase in enthalpy with increasing chain length.

For all four NAEs, three peaks were observed in either the first or second heating scan at 2.5 °C/min, two peaks occurring at temperatures below the crystal−isotropic liquid transition temperature, and one main peak corresponding to the crystal−isotropic liquid transition. Upon further heating/cooling cycles, the number of premelting peaks either increased or decreased. In addition, the number of premelting peaks was dependent on the solvent used during synthesis and recrystallization. In the case of stearoyl monoethanolamide, the first heating scan showed two additional peaks, while subsequent scans showed only one additional peak. These results are similar to what has been reported previously,[22,32] with the exception of lauroyl monoethanolamide which was shown to have only one premelting peak prior to the crystal−isotropic liquid transition. These premelting peaks are most likely attributed to crystal−crystal transitions. When observing melting of the neat lipid under the microscope, close to the pretransition temperatures recorded with DSC, changes in crystal shape and anisotropic polarization angle were observed (Figure 3). Our group has reported similar crystal−crystal associated transitions for saturated alkyl ureas.[36] Wouters et al. reported on polymorphisms in the crystal structure of stearoyl monoethanolamide. Evidence from X-ray crystallography indicated that the compound could exist in at least three polymorphic forms at distinct temperatures due to rearrangements of the hydrocarbon chains when heating the molecule.[32] They also demonstrated that the molecular packing of stearoyl monoethanolamide was similar to that of myristoyl monoethanolamide.[24,32] A similar study was recently performed on palmitoyl monoethanolamide, and, again, more than one polymorphic structure was detected, with molecular packing similar to the other two aforementioned saturated monoethanolamides[33] Thus, the premelting peaks observed for all of the molecules can most likely be attributed to different polymorphic forms of the crystal structures of the compounds.

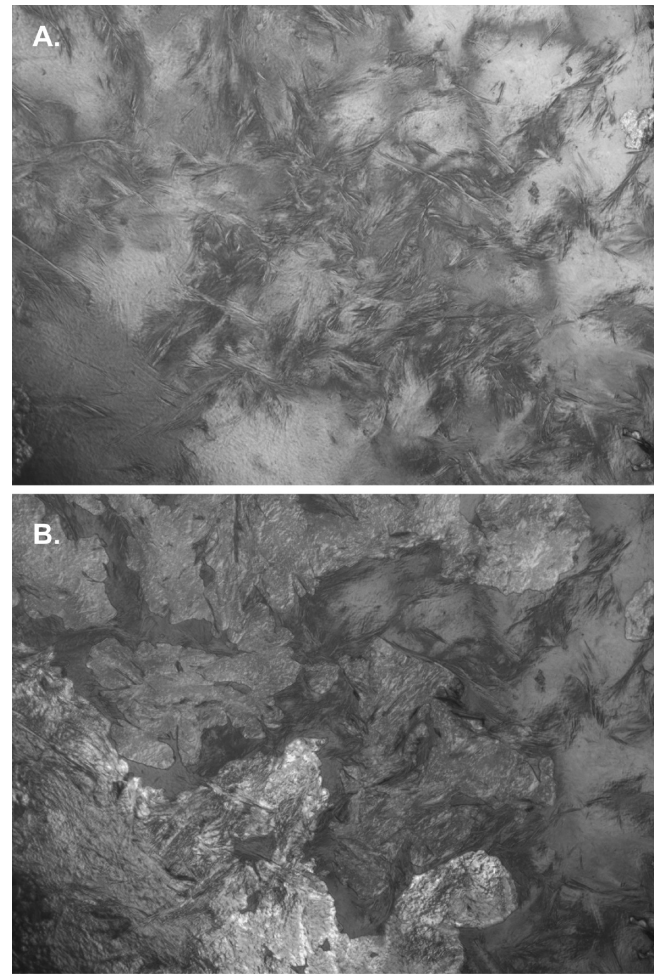

Figure 3. Optical microscopy of neat stearoyl monoethanolamide: (A) image acquired at 25 °C and (B) image acquired from same position at 85 °C. A polymorphic transition visible in the crystal structure occurs throughout parts of the lipid. This transition occurs at a similar temperature to a pretransition indicated by DSC.

XRD. The X-ray diffraction data obtained for the saturated monoethanolamide amphiphiles supports the existence of different crystalline polymorphic forms. The presence of multiple crystal structures is common for long chain compounds, due to different chain packing arrangements along with variations in chain tilt.[32] X-ray diffraction patterns for lauroyl, myristoyl, palmitoyl, and stearoyl monoethanolamide are shown in Figure

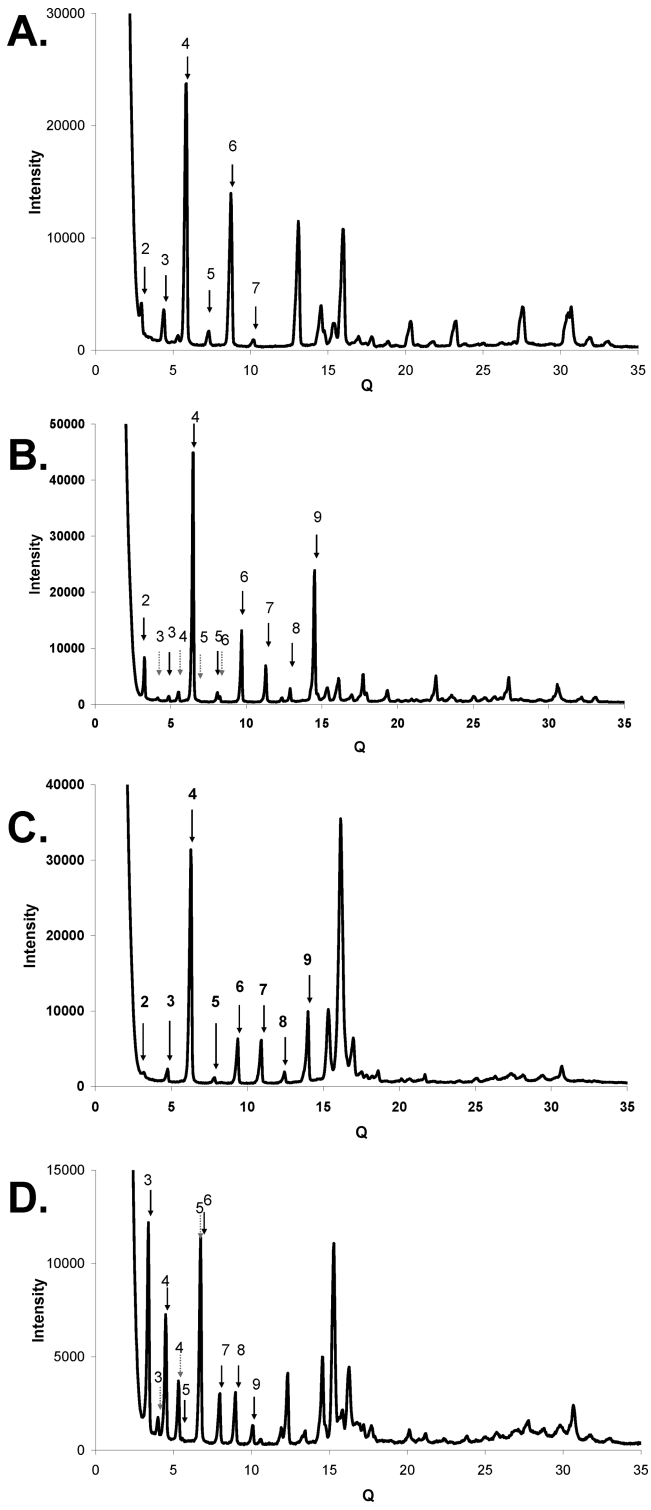

Figure 4. XRD of saturated monoethanolamide lipids at room temperature: (A) lauroyl monoethanolamide, (B) myristoyl monoethanolamide, (C) palmitoyl monoethanolamide, and (D) stearoyl monoethanolamide. Arrows indicate lamellar spacing for two different polymorphs of myristoyl and stearoyl monoethanolamide and one polymorph of lauroyl and palmitoyl monoethanolamide.

4A−D, respectively. All four saturated monoethanolamide lipids have diffraction patterns consistent with lamellar packing. The *d*-spacing of each crystal structure was calculated from the location of the peaks within the XRD pattern. In all cases, seven or more peaks were used to confirm the main crystal structure present. In addition to the peaks corresponding to the major crystal form, the myristoyl, palmitoyl, and stearoyl monoethanolamide XRD patterns all contained a second series of regularly repeating peaks indicating the existence of a second polymorphic crystal structure. Fewer peaks corresponding to the second polymorph were resolved due to lower peak intensity; however, at least three peaks were used to confirm the presence of a second distinct lamellar crystal structure. The existence of multiple polymorphs is supported by DSC results which show one to two small premelting transitions, attributed to crystal−crystal transitions, as well as optical visualization of crystal birefringence changes at temperatures corresponding to these DSC pretransitions. The second polymorph is likely to be more prevalent at temperatures above room temperature, but it is still observed in smaller quantities at room temperature.

TABLE 2: Lattice Parameters Determined from XRD Data for Saturated Monoethanolamide Surfactants

surfactant	polymorph 1	polymorph 2
stearoyl monoethanolamide	47.1 Å	55.9 Å
palmitoyl monoethanolamide	42.8 Å	50.7 Å
myristoyl monoethanolamide	38.5 Å	45.5 Å
lauroyl monoethanolamide		39.7 Å

The *d*-spacing for the crystal structures of the four lipids is shown in Table 2. For stearoyl, palmitoyl, and myristoyl monoethanolamide, polymorph 1, which is the dominant polymorph, displays an increase of 4.3 Å per increase of 2 C in the chain length. A similar trend is noted for polymorph 2, but with a 5.2 Å increase per increase of 2 C in chain length. For lauroyl monoethanolamide, the single *d*-spacing observed is 5.8 Å less than that seen for polymorph 2 of myristoyl monoethanolamide. Thus, it is likely that the lamellar crystalline structure of lauroyl monoethanolamide at room temperature is more closely related to polymorph 2. Similar molecular structure, packing, and intermolecular interactions have been previously demonstrated for myristoyl, palmitoyl, and stearoyl monoethanolamide.[24,32,33] The lattice parameters displayed here for both myristoyl and stearoyl monoethanolamide are the same as those reported in the literature.[24,32] However, the value we have obtained for the lattice parameter of palmitoyl monoethanolamide is slightly lower than that reported in the literature. The polymorphic structure exhibited by a crystal is dependent on the sample history and solvent crystallization method, and thus could account for the observed difference in lattice parameter for palmitoyl monoethanolamide.

Water Penetration into Saturated Monoethanolamide Lipids. Water-penetration studies of the solid material may provide information on the lyotropic phase behavior of lipid systems. As water penetrates into the neat lipid, a concentration gradient may be created. As long as the crystal solubility (CST) or Krafft temperature is attained, liquid crystalline phases may be observed. Due to the relatively high temperatures at which phase transitions occur for these four amphiphiles, water penetration was used as the sole indicator of lyotropic behavior as other, more quantitative techniques, such as binary phase behavior studies and small-angle X-ray scattering (SAXS), proved impractical. The highly hydrophobic nature of the four saturated monoethanolamides combined with the fact that lyotropic phases only formed at high temperatures (ranging from 65 to 100 °C) proved detrimental to obtaining even partial binary phase diagrams. Rapid water evaporation followed by water condensation above the lipid even in sealed containers combined with the inability of these lipids to equilibrate properly at these high temperatures even over long periods of time presented a major obstacle in obtaining a high temperature phase diagram of such a complex system. Very few studies have successfully

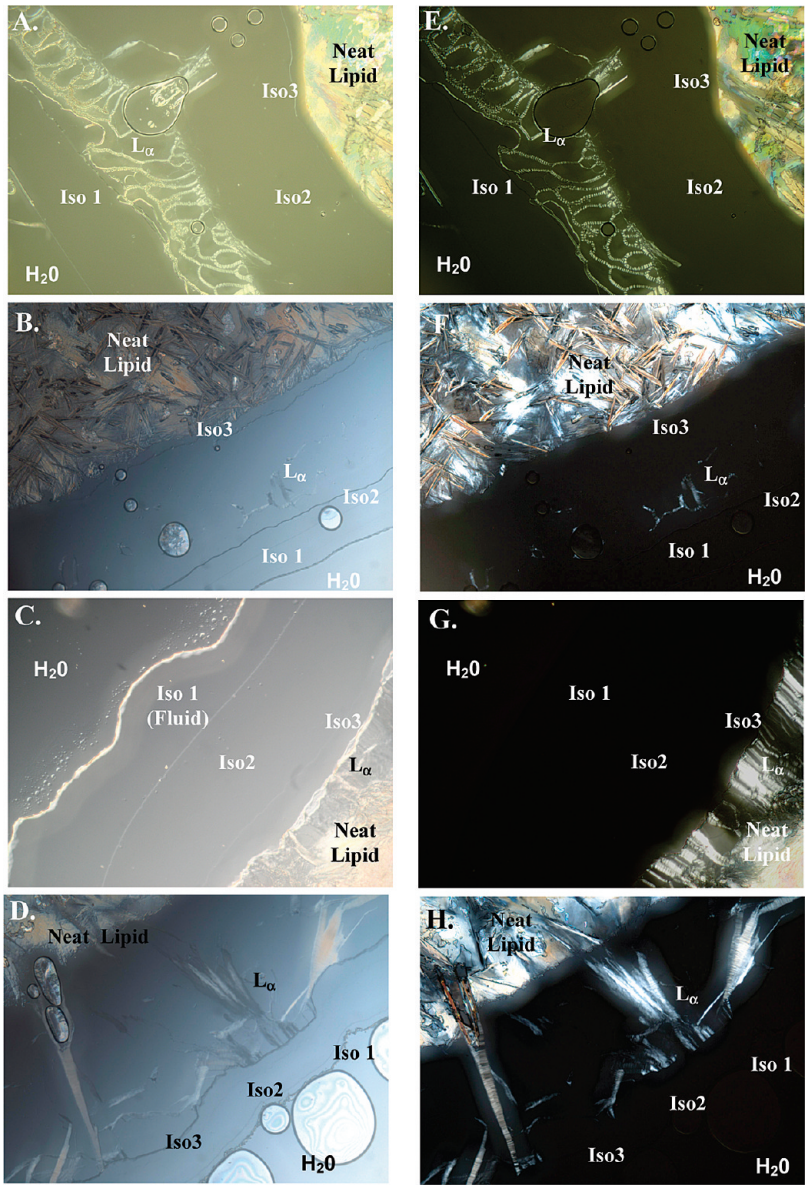

Figure 5. Optical microscopy without (A−D) and with (E−H) crossed polarizers of water penetration of lauroyl monoethanolamide at 70 °C (A,E); myristoyl monoethanolamide at 75 °C (B,F); palmitoyl monoethanolamide at 80 °C (C,G); and stearoyl monoethanolamide at 90 °C (D,H).

TABLE 3: Phases Observed via Optical Microscopy and the Temperatures at Which They Appear

lipid	lamellar	isotropic	isotropic melt
stearoyl monoethanolamide	87−100 °C	3 isotropic, 87−92.5 °C 4 isotropic, 92.5−100 °C	100−102.5 °C
palmitoyl monoethanolamide	80−85 °C	3 isotropic, 80−85 °C	85−90 °C
myristoyl monoethanolamide	70−75 °C	3 isotropic, 70−80 °C 2 isotropic, 85 °C	85−90 °C
lauroyl monoethanolamide	65−75 °C	3 isotropic, 65−80 °C	80−85 °C

obtained proper phase diagrams for high temperature systems due to similar difficulties.

Water penetration data obtained for all four saturated NAEs showed interesting liquid crystalline behavior (Figure 5). For all four compounds, at least three isotropic phases were observed in the higher temperature, lower lipid concentration range. In addition, all four displayed an anisotropic phase. Table 3 summarizes the phases observed and the temperatures at which they were observed for each compound. The lyotropic liquid crystalline phases begin to form at temperatures lower than the melting point, and the temperature at which liquid crystalline phase formation is observed decreases with decreasing hydrocarbon chain length, in a similar manner to the melting point. A previous study by Ramakrishnan et al. demonstrated the possible existence of a liquid crystalline phase in even chain length saturated monoethanolamides (C8−C20) via DSC of saturated monoethanolamides in excess water.[22] The reported temperature at which the observed transition occurs is almost identical to the temperatures at which we observed initial lyotropic phase formation as indicated in Table 3.

The same anisotropic texture is visualized for all four different monoethanolamide lipids and corresponds to a classic L_α phase

TABLE 4: Average Solid Lipid Nanoparticle Diameter and Polydispersity Index (PDI) over Time for Palmitoyl Monoethanolamide Dispersions

	average size (d.nm)	PDI
7 days	474.5	0.202
14 days	473.4	0.186
25 days	491.5	0.207

texture. However, while an obvious L_α phase is seen for both lauroyl (Figure 5A,E) and palmitoyl monoethanolamide (Figure 5B,F), a fully equilibrated L_α band was not apparent for either myristoyl (Figure 5C,G) or stearoyl monoethanolamide (Figure 5D,H). In the case of these two lipids, a small amount of the L_α texture could be seen within an isotropic band indicating an unequilibrated phase. Due to the high temperatures at which these phases form, the inability to equilibrate is most likely attributed to rapid water evaporation preventing full equilibration of the phase.

In the absence of diffraction data, it is impossible to definitively assign phase types to the several isotropic phases. However, in some cases, visual inspection was adequate to assign an isotropic phase as highly viscous or fluid. We therefore speculate on phase identity, based on other similar systems, the phase formation of an "ideal system," and the molecular constraints of the four molecules examined.

The phase sequences for palmitoyl, myristoyl, and stearoyl monoethanolamide are very similar (Figure 5) and adopt the following sequence with increasing water content: isotropic−lamellar−two or three isotropic bands. We attribute this to the phase sequence inverse micelles (L_2)−lamellar (L_α)−inverse cubic−water, similar to previously published phase diagrams for a variety of other amphiphile/water systems.[14,37,38] The narrow isotropic band displayed by myristoyl monoethanolamide next to the neat lipid (i.e., at low water content), attributed to an L_2 micellar phase, is observed throughout the full temperature range for liquid crystalline formation. However, for stearoyl monoethanolamide, a similar low water content isotropic band corresponding to a possible L_2 phase was observed only at temperatures above 92.5 °C. An isotropic band at the lowest water content was not observed for palmitoyl monoethanolamide, possibly reflecting issues with high temperature and rapid water evaporation. As the water content increases, a liquid crystalline L_α phase is visible for the three above-mentioned lipids, followed by two-three isotropic bands. These isotropic bands appear to be quite viscous and thus may correspond to inverse cubic phases. Three types of inverse cubic phase have been identified in lipid systems. These are based on the Schwarz diamond (D) and primitive (P) and on the Schoen gyroid (G) minimal surfaces and are denoted Q_{II}^D, Q_{II}^P, and Q_{II}^G respectively. In order of increasing water content, the cubic phases observed would likely correspond to $Q_{II}^G-Q_{II}^D-Q_{II}^P$.[39]

A different phase order was observed for lauroyl monoethanolamide, namely (from low to high water concentration), viscous isotropic (bubbles are effectively "stuck" in place), L_α, and fluid isotropic (could be seen flowing quickly around the outside of the other phases). It is possible that the shorter lauroyl chain results in the formation of normal phases instead of the putative inverse phases formed by the other three lipids. These results, however, were unable to be confirmed by either binary phase studies or SAXS due to the high temperature nature at which the phases formed.

Solid Lipid Nanoparticle Dispersions. High pressure homogenization of palmitoyl monoethanolamide in water resulted in a dispersion of SLNs that possessed an opaque, milky white appearance. The SLNs had a relatively uniform size distribution with a PDI $\sim$ 0.200 and an average size of 480 $\pm$ 10 nm (Table 4). The average size and distribution of the SLNs remained stable over the course of 3 weeks (Figure 6).

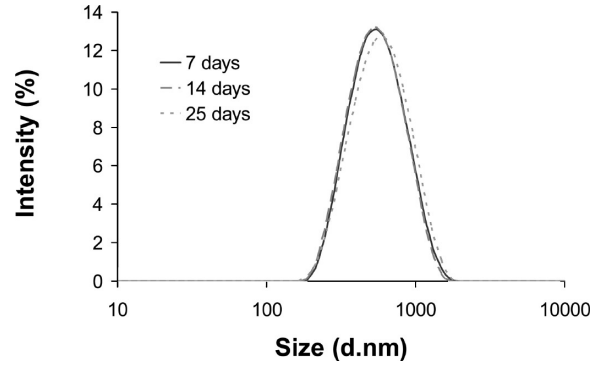

Figure 6. Diameter size distribution of palmitoyl monoethanolamide solid lipid nanoparticles over time.

For visualization by cryo-TEM, samples were prepared on two different types of carbon grids: C-flat, which has regular, 2 μm diameter, circular holes, and lacey, which has random holes. The average size of the imaged particles was in good agreement with the data obtained on the nanosizer; however, some of the imaged particles were up to 1 μm in size. The shape of the particles varies from very thin, geometric crystals to more solid, 3-D-looking particles, still crystalline, but with more rounded edges (Figure 7). Furthermore, the particles are all quite radiation-sensitive, and damage occurred at a very low electron dose (<70 electrons/nm^2; the usual low-dose criterion is <1000 electrons/nm^2).

Cytotoxicity of SLNs. In the development of a drug delivery system, it is vital to assess the inherent toxicity of the vehicle. Currently, the mechanism behind nanoparticle induced toxicity is not well understood. *In vitro* nanoparticle toxicity can be affected by the size, internal nanostructure, and molecular composition of the particle and thus can vary greatly from the toxicity exhibited by the same compound in bulk form. Therefore, the *in vitro* toxicity of the palmitoyl monoethanolamide SLNs was evaluated in both healthy HMEpiC and MCF7 cancer cells. Cells were incubated for 48 h with SLNs ranging in concentration from 0.003 to 30 mM. The SLNs only displayed a low level of toxicity toward either the HMEpiC or MCF7 cells at extremely high concentrations (3 mM and above) with the MCF7 population being reduced by 20−30%, while the HMEpiC population was reduced by less than 15% of the initial population (Figure 8). These concentration levels are on the order of 1000−10 000-fold greater than IC_{50} values (concentration that results in 50% cell death) for chemotherapeutic drug levels.[40,41]

Due to the endogenous nature of bulk palmitoyl monoethanolamide, the inherent biological function has been examined in a number of different studies. These studies have indicated that, alone, bulk palmitoyl monoethanolamide by itself is not highly toxic and does not effect cellular proliferation of various cancer cell lines including MCF7 at concentrations up to 10 μM. In contrast, anandamide, a widely studied unsaturated NAE, displays a cytotoxic effect on these same cancer cell lines at concentrations well below 10 μM.[20,42−45] It is believed that cannabinoid receptor 1 (CB_1) plays a vital role in the antiproliferative effect of anandamide. However, palmitoyl monoethanolamide does not bind with any affinity to CB_1; thus, it is not surprising that high concentrations would fail to elicit the same response.[43−45] Instead, studies have demonstrated the role

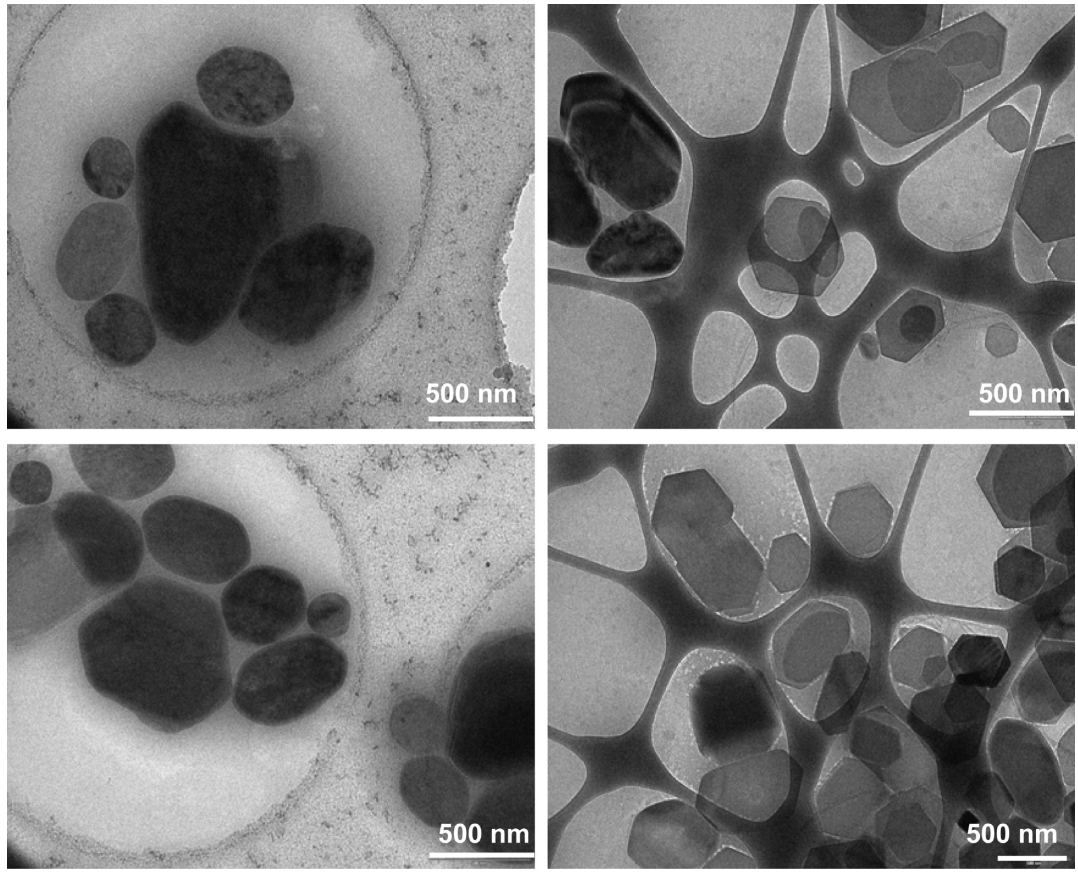

Figure 7. Cryo-TEM images of palmitoyl monoethanolamide solid lipid nanoparticles.

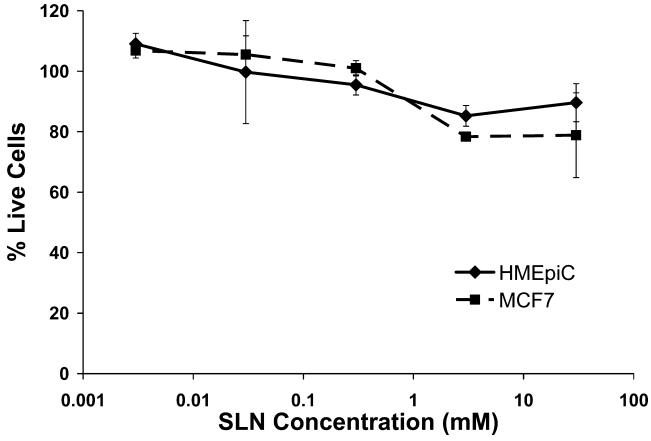

Figure 8. Toxicity of palmitoyl monoethanolamide solid lipid nanoparticles.

of PEA as an entourage or synergistic molecule in enhancing the antiproliferative effect of both anandamide and vanilloid receptor 1 agonists.[20,44,45]

Here, we have demonstrated that when palmitoyl monoethanolamide is delivered in a SLN form, concentrations 1000-fold greater than those indicated in the literature have little effect on both MCF7 and HMEpiC. The SLN formulation allows for delivery of higher concentrations than would be possible with the bulk crystalline form alone and thus allows for examination of the effect of higher concentrations of palmitoyl monoethanolamide than previously reported. In addition, the nature and stability of the colloidal particles in solution prevents bombardment with large quantities of the molecule all at once, and instead the particles are more likely to exhibit a prolonged, slow release of the individual palmitoyl monoethanolamide molecules, thereby exposing the cells to concentrations that are effectively much lower than the actual concentration present over a 48 h period. Moreover, this type of formulation could potentially be utilized for encapsulation and slow release of a variety of therapeutically relevant hydrophilic, hydrophobic, or amphiphilic molecules, or provide a means of reducing the systemic toxicity while delivering high payloads of more toxic drugs. More in depth studies are necessary to evaluate both the effect of long-term delivery of high concentrations of palmitoyl monoethanolamide as well as the SLNs' potential as delivery vehicles for other therapeutics.

Conclusions

The current study has demonstrated the ability of nonionic monoethanolamide lipids with saturated hydrocarbon chains to form lyotropic liquid crystalline phases at temperatures ranging from 65 to 100 °C. At high temperatures, such as these, it is likely that the saturated crystalline chains become fluid, thereby resulting in an effective increased hydrocarbon volume. The large occupied chain volume combined with the small polar monoethanolamide headgroup restricts the packing ability of the amphiphiles and results in the effective wedge-shaped conformation necessary for inverse phase formation. Saturated lipids examined in this study displayed an L_α phase in addition to at least two isotropic phases. Although the precise identity of these isotropic phases was not unambiguously determined, optical observation of the isotropic bands showed that some were quite stiff, indicating the likely presence of inverse bicontinuous cubic phases. This would be consistent with previously published phase diagrams on similar amphiphiles including unsaturated and isoprenoid-type monoethanolamide amphiphiles.[13,14]

Solid lipid nanoparticles were made from lamellar crystalline palmitoyl monoethanolamide and were stable over at least a 3 week period. The formation of these nanoparticles can allow for ease of administration of high concentrations of this endogenous amphiphile. Furthermore, toxicity studies revealed that, even at a concentration of 30 mM, which is much higher than examined or reported in the literature, palmitoyl monoethanolamide solid lipid nanoparticles had little effect on normal human mammary epithelial cells and human breast cancer cells, HMEpiC and MCF7, respectively. Consequently, solid lipid nanoparticles based on saturated nonionic monoethanolamide lipids represent a prospective series of nanostructured self-assembly materials that may be suitable for a range of encapsulation and controlled release applications.

Acknowledgment. C.J.D. is the recipient of an Australian Research Council Federation Fellowship.

References and Notes

(1) Brenner, R. R. *Prog. Lipid Res.* **1984**, *23*, 69.
(2) Misquitta, Y.; Caffrey, M. *Biophys. J.* **2001**, *81*, 1047.
(3) Seddon, J. M.; Squires, A. M.; Conn, C. E.; Ces, O.; Heron, A. J.; Mulet, X.; Shearman, G. C.; Templer, R. H. *Philos. Trans. R. Soc. London, Ser. A* **2006**, *364*, 2635.
(4) Drummond, C. J.; Fong, C. *Curr. Opin. Colloid Interface Sci.* **1999**, *4*, 449.
(5) Engstrom, S. *Abstr. Pap. Am. Chem. Soc.* **1990**, *200*, 45.
(6) Boulikas, T. *Oncol. Rep.* **1996**, *3*, 989.
(7) Lasic, D. D. *J. Controlled Release* **1997**, *48*, 203.
(8) Landau, E. M.; Rosenbusch, J. P. *Proc. Natl. Acad. Sci. U.S.A.* **1996**, *93*, 14532.
(9) Ostermeier, C.; Michel, H. *Curr. Opin. Struct. Biol.* **1997**, *7*, 697.
(10) Rummel, G.; Hardmeyer, A.; Widmer, C.; Chiu, M. L.; Nollert, P.; Locher, K. P.; Pedruzzi, I.; Landau, E. M.; Rosenbusch, J. P. *J. Struct. Biol.* **1998**, *121*, 82.
(11) Israelachvili, J. N.; Mitchell, D. J.; Ninham, B. W. *J. Chem. Soc., Faraday Trans.* **1976**, *72*, 1525.
(12) Kaasgaard, T.; Drummond, C. J. *Phys. Chem. Chem. Phys.* **2006**, *8*, 4957.
(13) Sagnella, S. M.; Conn, C. E.; Krodkiewska, I.; Drummond, C. J. *Soft Matter* **2009**, *5*, 4823.
(14) Sagnella, S. M.; Conn, C. E.; Krodkiewska, I.; Moghaddam, M.; Seddon, J. M.; Drummond, C. J. *Langmuir*, published online Nov 20, http://dx.doi.org/10.1021/la903005q.
(15) Conn, C. E.; Ces, O.; Mulet, X.; Finet, S.; Winter, R.; Seddon, J. M.; Templer, R. H. *Phys. Rev. Lett.* **2006**, *96*, 108102.
(16) Mulet, X.; Gong, X.; Waddington, L. J.; Drummond, C. J. *ACS Nano* **2009**, *3*, 2789.
(17) Yang, L.; Huang, H. W. *Science* **2002**, *297*, 1877.
(18) Sheerin, A. H.; Zhang, T.; Saucier, D. M.; Corcoran, T. E. *Epilepsia* **2004**, *45*, 1184.
(19) Fong, C.; Wells, D.; Krodkiewska, I.; Hartley, P. G.; Drummond, C. J. *Chem. Mater.* **2006**, *18*, 594.
(20) De Petrocellis, L.; Bisogno, T.; Ligresti, A.; Bifulco, M.; Melck, D.; Di Marzo, V. *Fundam. Clin. Pharmacol.* **2002**, *16*, 297.
(21) Lo Verme, J.; Gaetani, S.; Fu, J.; Oveisi, F.; Burton, K.; Piomelli, D. *Cell. Mol. Life Sci.* **2005**, *62*, 708.
(22) Ramakrishnan, M.; Sheeba, V.; Komath, S. S.; Swamy, M. J. *Biochim. Biophys. Acta, Biomembr.* **1997**, *1329*, 302.
(23) Ramakrishnan, M.; Swamy, M. J. *Chem. Phys. Lipids* **1998**, *94*, 43.
(24) Ramakrishnan, M.; Swamy, M. J. *Biochim. Biophys. Acta, Biomembr.* **1999**, *1418*, 261.
(25) Sheskin, T.; Hanus, L.; Slager, J.; Vogel, Z.; Mechoulam, R. *J. Med. Chem.* **1997**, *40*, 659.
(26) Swamy, M. J.; Ramakrishnan, M.; Marsh, D.; Wurz, U. *Biochim. Biophys. Acta, Biomembr.* **2003**, *1616*, 174.
(27) Maccarrone, M.; Pauselli, R.; Di Rienzo, M.; Finazzi-Agro, A. *Biochem. J.* **2002**, *366*, 137.
(28) Maccarrone, M.; Cartoni, A.; Parolaro, D.; Margonelli, A.; Massi, P.; Bari, M.; Battista, N.; Finazzi-Agro, A. *Mol. Cell. Neurosci.* **2002**, *21*, 126.
(29) Terrazzino, S.; Berto, F.; Dalle Carbonare, M.; Fabris, M.; Guiotto, A.; Bernardini, D.; Leon, A. *FASEB J.* **2004**, *18*, 1580.
(30) Porter, A. C.; Felder, C. C. *Pharmacol. Ther.* **2001**, *90*, 45.
(31) Walker, J. M.; Krey, J. F.; Chu, C. J.; Huang, S. M. *Chem. Phys. Lipids* **2002**, *121*, 159.
(32) Wouters, J.; Vandevoorde, S.; Culot, C.; Docquir, F.; Lambert, D. M. *Chem. Phys. Lipids* **2002**, *119*, 13.
(33) Kamlekar, R. K.; Swamy, M. J. *J. Lipid Res.* **2006**, *47*, 1424.
(34) Bawarski, W. E.; Chidlowsky, E.; Bharali, D. J.; Mousa, S. A. *Nanomed.: Nanotechnol. Biol. Med.* **2008**, *4*, 273.
(35) Marcato, P. D.; Duran, N. *J. Nanosci. Nanotechnol.* **2008**, *8*, 2216.
(36) Wells, D.; Drummond, C. J. *Langmuir* **1999**, *15*, 4713.
(37) Barauskas, J.; Landh, T. *Langmuir* **2003**, *19*, 9562.
(38) Briggs, J.; Caffrey, M. *Biophys. J.* **1994**, *66*, 1263.
(39) Luzzati, V.; Tardieu, A.; Gulikkrz., T; Rivas, E.; Reisshus., F. *Nature* **1968**, *220*, 485.
(40) Guichard, S. M.; Macpherson, J. S.; Mayer, I.; Reid, E.; Muir, M.; Dodds, M.; Alexander, S.; Jodrell, D. I. *Eur. J. Cancer* **2008**, *44*, 310.
(41) Miwa, M.; Ura, M.; Nishida, M.; Sawada, N.; Ishikawa, T.; Mori, K.; Shimma, N.; Umeda, I.; Ishitsuka, H. *Eur. J. Cancer* **1998**, *34*, 1274.
(42) De Petrocellis, L.; Melck, D.; Bisogno, T.; Di Marzo, V. *Chem. Phys. Lipids* **2000**, *108*, 191.
(43) Di Marzo, V.; Melck, D.; De Petrocellis, L.; Bisogno, T. *Prostaglandins Other Lipid Mediators* **2000**, *61*, 43.
(44) Di Marzo, V.; Melck, D.; Orlando, P.; Bisogno, T.; Zagoory, O.; Bifulco, M.; Vogel, Z.; De Petrocellis, L. *Biochem. J.* **2001**, *358*, 249.
(45) Melck, D.; De Petrocellis, L.; Orlando, P.; Bisogno, T.; Laezza, C.; Bifulco, M.; Di Marzo, V. *Endocrinology* **2000**, *141*, 118.

JP910578H